Proc. Natl. Acad. Sci. USA
Vol. 95, pp. 4720–4725, April 1998
Neurobiology

R-type Ca^{2+} currents evoke transmitter release at a rat central synapse

LING-GANG WU*, J. GERARD G. BORST, AND BERT SAKMANN

Abteilung Zellphysiologie, Max-Planck-Institut für medizinische Forschung, Jahnstrasse 29, D-69120 Heidelberg, Germany

Contributed by Bert Sakmann, February 6, 1998

ABSTRACT **Voltage-dependent Ca^{2+} currents evoke synaptic transmitter release. Of six types of Ca^{2+} channels, L-, N-, P-, Q-, R-, and T-type, only N- and P/Q-type channels have been pharmacologically identified to mediate action-potential-evoked transmitter release in the mammalian central nervous system. We tested whether Ca^{2+} channels other than N- and P/Q-type control transmitter release in a calyx-type synapse of the rat medial nucleus of the trapezoid body. Simultaneous recordings of presynaptic Ca^{2+} influx and the excitatory postsynaptic current evoked by a single action potential were made at single synapses. The R-type channel, a high-voltage-activated Ca^{2+} channel resistant to L-, N-, and P/Q-type channel blockers, contributed 26% of the total Ca^{2+} influx during a presynaptic action potential. This Ca^{2+} current evoked transmitter release sufficiently large to initiate an action potential in the postsynaptic neuron. The R-type current controlled release with a lower efficacy than other types of Ca^{2+} currents. Activation of metabotropic glutamate receptors and γ-aminobutyric acid type B receptors inhibited the R-type current. Because a significant fraction of presynaptic Ca^{2+} channels remains unidentified in many other central synapses, the R-type current also could contribute to evoked transmitter release in these synapses.**

Biophysical and pharmacological analysis has led to the description of six classes of Ca^{2+} channels, usually referred to as L-, N-, P-, Q-, R-, and T-type (1, 2). Among them, N- and P/Q-type Ca^{2+} channels have been found to control transmitter release evoked by action potentials in most synapses examined so far (1, 2). In the presence of high concentrations of L-, N-, and P/Q-type channel blockers, a significant fraction (≈25%) of presynaptic Ca^{2+} channels remained unidentified at hippocampal (3) and cerebellar (4) synapses and in rat brain synaptosomes (5). These unidentified channels could be of R- or T-type. However, it has not been shown unequivocally that action potentials evoke transmitter release in the presence of saturating concentrations of L-, N-, and P/Q-type channel blockers (3, 4), even when release was enhanced by a train of stimulations (6) or by the K^+ channel blocker 4-aminopyridine (7). In several other studies, combined application of the N-type channel blocker ω-conotoxin-GVIA and the P/Q-type blocker ω-agatoxin-IVA did not completely block synaptic transmission (8–10). In these studies, however, the concentration of ω-agatoxin-IVA was at most 100–200 nM, which is not sufficient to completely block Q-type channels (11, 12). In brief, whether Ca^{2+} channels other than N- and P/Q-type participate in controlling action-potential-evoked transmitter release is not known.

Recently, simultaneous presynaptic and postsynaptic recordings were made at single calyx-type synapses in rat medial nucleus of the trapezoid body (MNTB) (13, 14). At this axosomatic synapse, voltage control can be obtained for both the presynaptic Ca^{2+} current and the excitatory postsynaptic current (EPSC) (13, 15, 16). The large amplitude of the EPSC makes it very suitable for testing the effect of Ca^{2+} channel blockers on synaptic transmission. We used this synapse to test whether Ca^{2+} channels other than N- and P/Q-type are involved in action-potential-evoked synaptic transmission at the level of a single synapse. We found that about one-quarter of the presynaptic Ca^{2+} current is contributed by the R-type Ca^{2+} channel. This channel controls transmitter release with a lower efficacy than other types of Ca^{2+} channels.

METHODS

Electrophysiology. Slices were cut from the brainstem of 8- to 10-day-old Wistar rats, transferred to a recording chamber, and perfused at room temperature (23–24°C) with a solution containing: 125 mM NaCl, 2.5 mM KCl, 1 mM $MgCl_2$, 2 mM $CaCl_2$, 25 mM dextrose, 1.25 mM NaH_2PO_4, 0.4 mM ascorbic acid, 3 mM *myo*-inositol, 2 mM sodium pyruvate, 25 mM $NaHCO_3$, pH 7.4 when bubbled with 95% O_2, 5% CO_2 (13). Whole-cell current clamp recordings from terminals were made with an AxoClamp-2B amplifier (Axon Instruments) and glass pipettes (8–12 MΩ) containing: 115 mM potassium gluconate, 20 mM KCl, 4 mM MgATP, 10 mM Na_2-phosphocreatine, 0.3 mM GTP, 10 mM Hepes, 0.05 mM fura-2 (Molecular Probes), pH 7.2, adjusted with KOH. Whole-cell voltage clamp recordings from postsynaptic cells were made with an Axopatch-200A amplifier. Pipettes had a resistance of 1.5–2 MΩ and were filled with the same solution as the pipettes used for presynaptic recordings, except they contained 0.5 mM EGTA instead of 50 μM fura-2. Series resistance in postsynaptic recordings (<15 MΩ) was always compensated to 98% (lag 10 μs).

Whole-cell Ca^{2+} current recordings from terminals were made with an Axopatch-200A amplifier and pipettes with a resistance of 4–6 MΩ that contained the same intracellular solution as used for current clamp recordings except that potassium was replaced by cesium. In addition, 1 μM tetrodotoxin and 0.1 mM 3,4-diaminopyridine (Sigma) were added to the extracellular solution and 20 mM NaCl was replaced with 20 mM tetraethylammonium chloride (Sigma) to block sodium and potassium channels (13). Unless mentioned otherwise, 2 mM Ca^{2+} was used as the charge carrier. Series resistance (<35 MΩ) compensation was set at 90%, with a lag of 10 μs, prediction was set at 60%. Subtraction of the passive response was by the P/-5 method. Terminals with a capacitance of less than 35 pF were selected to avoid long axons (16). The fura-2 fluorescence image was used to confirm the presynaptic origin of the recording at the end of the experiment. For the waveform command, we used the presynaptic

The publication costs of this article were defrayed in part by page charge payment. This article must therefore be hereby marked "*advertisement*" in accordance with 18 U.S.C. §1734 solely to indicate this fact.

Abbreviations: MNTB, medial nucleus of the trapezoid body; EPSC, excitatory postsynaptic current; MVIIC, ω-conotoxin-MVIIC; $I_{Ca(AP)}$, Ca^{2+} currents evoked by an action potential waveform command; $GABA_B$, γ-aminobutyric acid type B.

*To whom reprint requests should be addressed. e-mail: lgwu@sunny.mpimf-heidelberg.mpg.de.

action potential displayed in figure 2A of ref. 13, interpolated to 20 μs per point with a cubic spline. Potentials were corrected for a liquid junction potential of −11 mV between the extracellular and the pipette solution. Holding potential for voltage-clamp experiments was −80 mV, unless noted otherwise. Potentials or currents were low-pass filtered at 2–5 kHz and digitized at 20–50 kHz with a 16-bit analogue-to-digital converter (Instrutech, Greatneck, NY).

Optical Recordings. The optical recording system was comprised of an upright epifluorescence microscope (Axioskop, Achroplan 40×, numerical aperture 0.75, Zeiss), equipped with a polychromatic illumination system (T.I.L.L. Photonics, Munich, Germany), a dichroic mirror (410 nm), a long pass (415 nm) emission filter, and two photodiodes on the image plane for signal and background subtraction, respectively (17). Excitation light was coupled to the microscope via a light guide. Fura-2 measurements of Ca^{2+} concentration were made by forming ratios between recordings (100–500 ms) of fluorescence (after background subtraction) at excitation wavelengths of 357 nm (isosbestic) and 380 nm (18). R_{max} and R_{min}, the parameters used for calculating Ca^{2+} concentrations, were obtained from *in situ* calibrations as described in ref. 19. A value of 273 nM for the K_d of fura-2 measured *in situ* was taken from ref. 19. Fluorescence signals recorded by a photodiode (Hamamatsu, Hamamatsu City, Japan) were filtered at 30 Hz (8-pole Bessel filter). Because the Ca^{2+} transient evoked by an action potential decays with a time constant of more than 400 ms in the presence of 50 μM fura-2 (19), filtering this transient at 30 Hz did not affect the measurement of its amplitude. Fura-2 was far from saturation during single action potentials, because (*i*) the peak Ca^{2+} concentrations evoked by single action potentials were usually less than the K_d of fura-2 measured *in situ* (19), and (*ii*) paired-pulse-action-potential stimulation (interval: 50 ms) caused approximately the same Ca^{2+} influx for each action potential (not shown).

For simultaneous presynaptic and postsynaptic recordings, only synapses in which the postsynaptic cells discharged an action potential in response to afferent stimulation were selected for recording (13). Single afferent stimuli were given via a bipolar electrode (3–30 V, 100 μs) placed at the midline of the trapezoid body. Stimulation interval was 20–30 sec.

Pharmacology. The effect of a toxin was evaluated after it reached equilibrium (e.g., Fig. 1*A*). Data are expressed as mean ± SEM. If not mentioned in the text, the concentrations of ω-conotoxin-MVIIC (MVIIC) (Research Biochemicals, Natick, MA), ω-conotoxin-GVIA (Bachem), ω-agatoxin-IVA (a gift from N.A. Saccomano, Pfizer) and $NiCl_2$ were 8 μM, 1 μM, 100 nM, and 100 μM, respectively. The metabotropic glutamate receptor agonist L-AP4 was purchased from Tocris Neuramin (Bristol, U.K.). The γ-aminobutyric acid type B ($GABA_B$) receptor agonist (R)-(−)-baclofen was a gift from CIBA–Geigy. The toxins did not significantly affect the resting membrane potential, the action potential, and the resting Ca^{2+} concentration of the terminal (e.g., Fig. 1*B*). The toxins were applied in the presence of 0.1 mg/ml cytochrome *c* to block nonspecific binding sites. Cytochrome *c* did not significantly affect the EPSC ($n = 16, P > 0.5$), or presynaptic Ca^{2+} influx ($n = 3, P > 0.5$). Statistical significance was tested with a paired *t* test, unless noted otherwise.

RESULTS AND DISCUSSION

Ca^{2+} Channels Other Than L-, N-, and P/Q-Type Contribute to Synaptic Transmission. We studied the effect of different Ca^{2+} channel blockers on synaptic transmission in rat MNTB synapses in acute brainstem slices. Presynaptic action potentials were evoked by electrical stimulation of the afferent axon via a bipolar electrode positioned at the midline of the trapezoid body. Presynaptic Ca^{2+} influx ($\Delta[Ca^{2+}]$) was quantified with the Ca^{2+} indicator fura-2. Transmitter release was monitored by measuring the amplitude of the EPSC. Application of 8 μM MVIIC, a blocker of N- and P/Q-type Ca^{2+} channels (20, 21), reduced the $\Delta[Ca^{2+}]$ to 26 ± 1% ($n = 9$) and the EPSC to 0.8 ± 0.1% ($n = 7$, Fig. 1*A*). This effect was reached about 10 min after the toxin application (Fig. 1*A*) and was largely irreversible during a washout period of up to 45 min

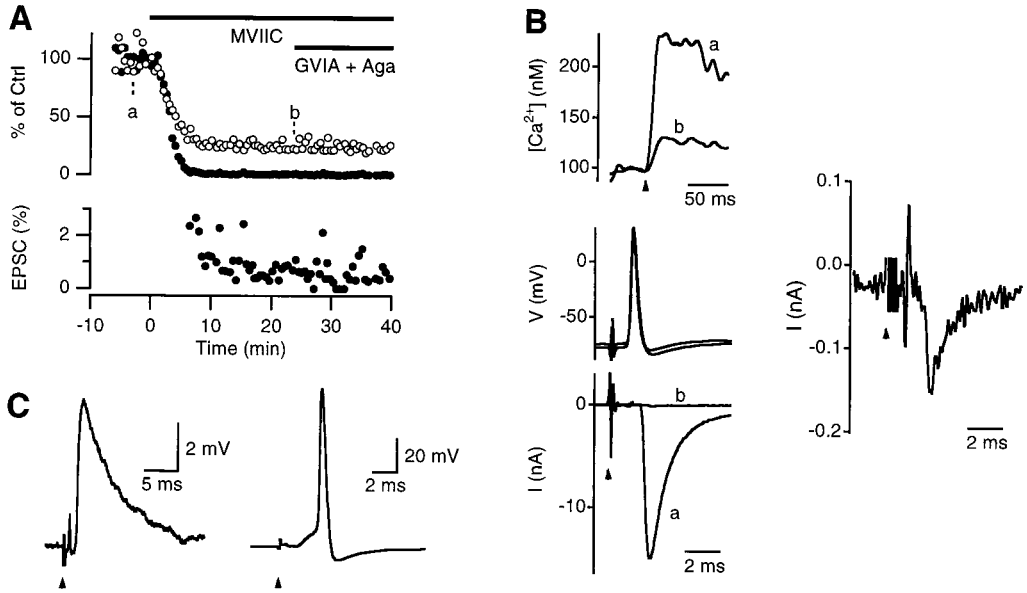

FIG. 1. The MVIIC-insensitive Ca^{2+} channel mediates action-potential-evoked transmitter release. (*A*) MVIIC (8 μM) reduced both the $\Delta[Ca^{2+}]$ (○) and the EPSC (●) evoked by a single action potential. Additional application of ω-conotoxin-GVIA (GVIA, 1 μM) and ω-agatoxin-IVA (Aga, 100 nM) did not further reduce either the $\Delta[Ca^{2+}]$ or the EPSC. The EPSC was clearly not abolished, as shown on a different amplitude scale (*Lower*). (*B*) Sample recordings of the presynaptic Ca^{2+} influx (*Upper*), presynaptic action potentials and the EPSCs (*Lower*) before (a) and after (b) MVIIC application, as indicated in *A*. The EPSC trace b was plotted on a different scale in the right. Arrow heads point to the time at which the stimulus was given (same for *C*). Stimulation artifacts were truncated (same for *C*). Note that each sample recording was taken from a single sweep (the same as in all the following figures). (*C*) Sample recordings of sub-threshold (*Left*) and supra-threshold (*Right*) excitatory postsynaptic potentials in the presence of MVIIC from a different principal cell. The resting membrane potential was −74 mV.

(not shown). Because of the large size of the EPSC (>2 nA) in control solution, the EPSC that remained after MVIIC application was well resolved (Fig. 1 *A*, *Lower*, and *B*). This MVIIC-resistant synaptic current generated excitatory postsynaptic potentials, which often reached the threshold for initiation of an action potential in the postsynaptic neuron (Fig. 1*C*). These results show that the MVIIC-insensitive Ca^{2+} current evoked by a presynaptic action potential contributes to synaptic transmission.

The blocking effect of MVIIC was saturating at 8 μM, because application of high concentrations of the N-type channel blocker ω-conotoxin-GVIA (1 μM) and the P/Q-type blocker ω-Agatoxin-IVA (100 nM) did not further reduce either the $\Delta[Ca^{2+}]$ or the EPSC (Fig. 1*A*). Application of MVIIC alone, MVIIC+Aga+GVIA, or Aga+GVIA reduced $\Delta[Ca^{2+}]$ to 26 ± 1% (n = 9), 26 ± 2% (n = 8) or 27 ± 1% (n = 6), respectively. These blockers reduced the EPSC to 0.8 ± 0.1% (n = 7), 0.9 ± 0.2% (n = 4), or 0.7 ± 0.1% (n = 4), respectively. These effects were not significantly different ($P > 0.5$, ANOVA). In the presence of 8 μM MVIIC, addition of another 8 μM MVIIC did not further reduce the $\Delta[Ca^{2+}]$ significantly (n = 3, $P > 0.5$, data not shown). Application of high concentrations of the L-type channel blockers nimodipine (10 μM) or nifedipine (10 μM) did not significantly change either the $\Delta[Ca^{2+}]$ (n = 3, $P >$ 0.5) or the EPSC ($n = 3, P > 0.5$, data not shown), suggesting that L-type Ca^{2+} channels are not present in the terminal. We conclude that presynaptic Ca^{2+} currents resistant to L-, N-, and P/Q-type blockers can be isolated by application of 8 μM MVIIC.

Recently, we found that the MVIIC-sensitive channels at the terminal of the MNTB synapse are subdivided into ω-conotoxin-GVIA sensitive N-type and ω-agatoxin-IVA sensitive P/Q-type channels (36). These two types of channels colocalize with MVIIC-insensitive channels at the same terminal (Fig. 1). These results are different from the results of Takahashi *et al.* (14), who found that on average 96% of the presynaptic Ca^{2+} current at the MNTB synapse is P/Q-type. The reason for this discrepancy is unknown.

About one-quarter of the presynaptic Ca^{2+} influx evoked by single action potentials is resistant to saturating concentrations of L-, N-, and P/Q-type channel blockers at hippocampal (3) and cerebellar (4) synapses. This unidentified Ca^{2+} influx does not evoke a clearly detectable synaptic response (3, 4, 6, 7). However, the signal-to-noise ratio of synaptic responses at these synapses was relatively low.

The Ca^{2+} Current Resistant to L-, N-, and P/Q-Type Blockers Is of R-Type. To study the gating, conductance, and pharmacological properties of MVIIC-insensitive Ca^{2+} channels, terminals were voltage-clamped and presynaptic Ca^{2+} currents were pharmacologically isolated (13). In control conditions, the threshold for current activation was at around −40 mV and the maximum current was reached at between −10 and 0 mV (Fig. 2*A*). At −30 to −20 mV, the current activation had a fast and a slow component (e.g., Fig. 2*A*, *Right*), the latter of which became faster at more depolarized potentials (16). MVIIC reduced the Ca^{2+} current at all potentials (Fig. 2*A*). The slow activation component at −30 to −20 mV was abolished (Fig. 2*A*, n = 9), indicating that the gating of MVIIC-sensitive and -insensitive currents is different. At a test potential of −10 mV, MVIIC reduced the Ca^{2+} current to 26 ± 3% (n = 9) of control, similar to its effect on the $\Delta[Ca^{2+}]$ during an action potential. Both activation ($\tau < 1$ ms at −10 mV) and deactivation ($\tau < 1$ ms at −80 mV) of the MVIIC-insensitive current were fast (Fig. 2*A*, see also Fig. 2*C* and Fig. 4).

During application of MVIIC, the effect of MVIIC was monitored by recording Ca^{2+} currents evoked by an action potential waveform command ($I_{Ca(AP)}$, Fig. 2*B*) (15). At equilibrium, MVIIC reduced the amplitude of the $I_{Ca(AP)}$ to 27 ± 4% (n = 3) without significantly affecting the waveform (measured as the half-width, $P > 0.3, n = 3$) of the $I_{Ca(AP)}$ (Fig. 2*B*). This effect is very similar to the effect of MVIIC on $\Delta[Ca^{2+}]$ (26 ± 1, n = 9), confirming that the fluorescence recording of $\Delta[Ca^{2+}]$ is proportional to the peak $I_{Ca(AP)}$ (17, 19).

Next, we studied the block of the MVIIC-insensitive current by $NiCl_2$ and $CdCl_2$. In the presence of MVIIC, 100 μM $NiCl_2$ reduced the MVIIC-insensitive current at all test potentials, but with a stronger block at the more hyperpolarizing test potentials (Fig. 2*C*). At −10 mV, the MVIIC-insensitive current was reduced to 46 ± 8% (n = 4) of control (Fig. 2*C*). Interestingly, even at 1 mM, $NiCl_2$ did not completely block the MVIIC-insensitive current (n = 3, Fig. 2*C*), suggesting that this current consists of two components, with one more sensitive to $NiCl_2$ than the other (see also ref. 22). The MVIIC-insensitive current was abolished by 50 μM $CdCl_2$ (n = 4, Fig. 2*C*).

The time course of inactivation of the MVIIC-insensitive current was studied with 2 mM Ba^{2+} rather than Ca^{2+} as the charge carrier to avoid possible Ca^{2+}-dependent channel inactivation. The holding potential was at −100 mV instead of at −80 mV in these experiments to minimize inactivation (see below). The Ba^{2+} current inactivated with a time constant of 38–51 ms (mean = 44 ± 3 ms, 8 terminals) to 53 ± 1% of the peak current at the end of 200 ms pulses ranging from −30 to 30 mV (Fig. 2*D*). The time constant and the percentage of the current remaining at the end of the voltage pulse were not significantly different between these test potentials ($P > 0.5$, ANOVA). Voltage-dependence of steady-state inactivation of the MVIIC-insensitive current showed two components with the midpoints of inactivation at −82 and −46 mV (n = 6), respectively, when 2 mM Ba^{2+} was the charge carrier (Fig. 2*E*). When Ca^{2+} was the charge carrier, the midpoints of inactivation of both components shifted 15 mV toward more positive potentials (n = 4, Fig. 2*E*).

In summary, the Ca^{2+} current resistant to L-, N-, and P/Q-type channel toxins activated at around −40 mV, peaked at around −10 to 0 mV, deactivated fast, inactivated fast with significant inactivation at negative potentials, and was relatively sensitive to $NiCl_2$ and $CdCl_2$. These properties are similar to those of the R-type current in granule neurons of the rat cerebellum (11, 12), and the currents of the class E recombinant Ca^{2+} channel (11, 23, 24), which presumably mediates the R-type current (11, 12). In addition, these properties show that the MVIIC-insensitive current is not a T-type current, because the latter activates at more negative potentials, deactivates slowly, and is relatively resistant to cadmium block (25–27). Therefore, the MVIIC-insensitive current in terminals of MNTB can be classified as an R-type current. The steady-state inactivation curve (Fig. 2*E*) and the incomplete block by nickel (Fig. 2*C*) suggest two components of the R-type current, but the results are also consistent with the different rates of inactivation and sensitivities to the block by nickel reported for R-type currents at different preparations (12, 22, 28) and for the class E recombinant Ca^{2+} channels coexpressed with different β subunits (23, 29, 30).

R-Type Ca^{2+} Channels Control Transmitter Release with a Lower Efficacy. Because the R-type current is sensitive to block by $NiCl_2$ (Fig. 2*C*), we examined whether $NiCl_2$ can be used as a selective blocker for the R-type current evoked by action potentials. The presynaptic Ca^{2+} influx evoked by single action potentials was recorded fluorometrically, and the effect of 100 μM $NiCl_2$ on $\Delta[Ca^{2+}]$ was compared in the absence and presence of MVIIC (Fig. 3*A*). The $\Delta[Ca^{2+}]$ was reduced by 21 ± 1% (n = 13) and 17 ± 1% (n = 7), respectively (Fig. 3*B*, percentages are all relative to the total $\Delta[Ca^{2+}]$ measured before addition of toxins). Thus, $NiCl_2$ preferentially blocked R-type current with only 19% (= (21 − 17)/21) of its effect being on the MVIIC-sensitive currents.

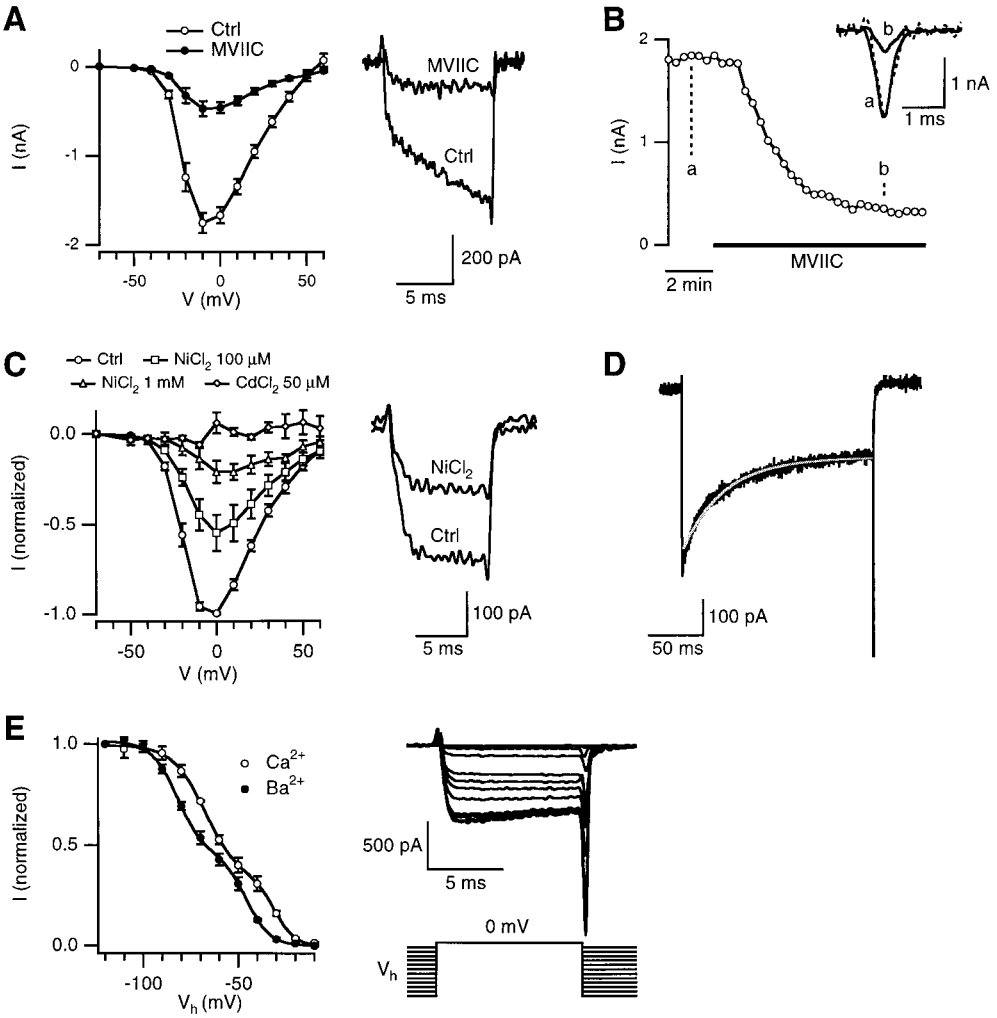

FIG. 2. The biophysical and pharmacological properties of the MVIIC-insensitive current. (*A*) Peak-current-voltage (*I–V*) relationship before (Ctrl) and after MVIIC (8 μM) application (*Left*, $n = 9$). Sample Ca^{2+} current recordings elicited at -30 mV before and after MVIIC application (*Right*). The holding potential was -80 mV with Ca^{2+} as the charge carrier (also in *B* and *C*). (*B*) Time course of the MVIIC block monitored by Ca^{2+} current evoked by an action potential waveform command. (*Inset*) Sample Ca^{2+} currents before (a) and after (b) MVIIC application. The dashed line is trace b scaled to trace a. (*C*) *I–V* relationship of the MVIIC-insensitive Ca^{2+} current before (ctrl) and after application of $NiCl_2$ (100 μM, $n = 4$; 1 mM, $n = 3$) or $CdCl_2$ (50 μM, $n = 4$). (*Right*) Sample currents elicited at -20 mV before (ctrl) and after application of 100 μM $NiCl_2$. The experiments were performed in the presence of MVIIC (same for *D* and *E*). (*D*) Time course of inactivation of the MVIIC-insensitive Ba^{2+} current. The current was elicited by a 200-ms pulse to $+10$ mV with 2 mM Ba^{2+} as the charge carrier (black trace). The inactivation time course was fit with a single exponential curve with a time constant of 43 ms (grayish white trace). (*E*) Voltage-dependence of inactivation of the MVIIC-insensitive Ba^{2+} ($n = 6$) and Ca^{2+} ($n = 4$) currents (*Left*). The current (*I*) was elicited from various holding potentials ($V_h = -120$ to -10 mV) to 0 mV, and was normalized with respect to the peak current elicited from $V_h = -120$ mV. (*Right*) An example with Ba^{2+} as the charge carrier. The interval between each test pulse was 30 sec. The grouped data (*Left*) was fit with a sum of two Boltzmann expressions: $I = C_1/\{1 + \exp[(V_h - V_{half1})/k_1]\} + (1 - C_1)/\{1 + \exp[(V_h - V_{half2})/k_2]\}$. When Ba^{2+} was the charge carrier, $C_1 = 0.56$, $V_{half1} = -82$ mV, $k_1 = 7$ mV, $V_{half2} = -46$ mV and $k_2 = 6$ mV. For Ca^{2+} as the charge carrier, $C_1 = 0.66$, $V_{half1} = -67$ mV, $k_1 = 9$ mV, $V_{half2} = -31$ mV and $k_2 = 5$ mV.

Using $NiCl_2$ as a selective blocker, we examined the efficacy of the R-type current in triggering release. The presynaptic $\Delta[Ca^{2+}]$ and the EPSC from single synapses were recorded simultaneously. $NiCl_2$ (100 μM) reduced both the $\Delta[Ca^{2+}]$ and the EPSC (Fig. 3*C*). The relation between the EPSC and the $\Delta[Ca^{2+}]$ (both in logarithmic scales) was fit with a linear regression line with a slope of 1.4 ± 0.1 ($n = 4$ pairs, Fig. 3*D*). In contrast, reducing the $[Ca^{2+}]_o$ from 2 to 1 mM (substituted with Mg^{2+}) resulted in a slope of 2.7 ± 0.2 ($n = 5$ synapses, Fig. 3 *E* and *F*), suggesting a cooperative mechanism for Ca^{2+} to trigger release (for review see refs. 1 and 31). The slope of 2.7 estimated here with paired recordings is lower than that determined by separate presynaptic and postsynaptic current recordings, which was about 4 (15). This difference is probably caused by some rundown of the EPSCs during recordings in which the EPSC amplitude was determined a long time (15–20 min) after the $[Ca^{2+}]_o$ was changed (15). On average, $NiCl_2$ reduced the EPSC by $36 \pm 4\%$ ($n = 4$). To estimate how much of this reduction is caused by a block of the MVIIC-sensitive current by $NiCl_2$, the efficacy of the MVIIC-sensitive current needs to be measured. A slope of 3.3 ± 0.3 was observed in three simultaneous recordings (e.g., Fig. 1*A*, slope = 3.6) in which MVIIC was applied (not shown). The high efficacy of the MVIIC-sensitive channels in triggering release is consistent with measurements in many other synapses (see ref. 31 for review). If $NiCl_2$ would reduce the EPSC only by inhibiting the MVIIC-sensitive current, it would reduce, on average, the EPSC by only 13% $(100\% - [100\% - (21\% - 17\%)]^{3.3})$. This is much smaller than the reduction of the EPSC by $NiCl_2$ that we observed (36%). Thus, R-type currents mediate action-potential-evoked transmitter release to a significant amount, but with a lower efficacy than other Ca^{2+} currents.

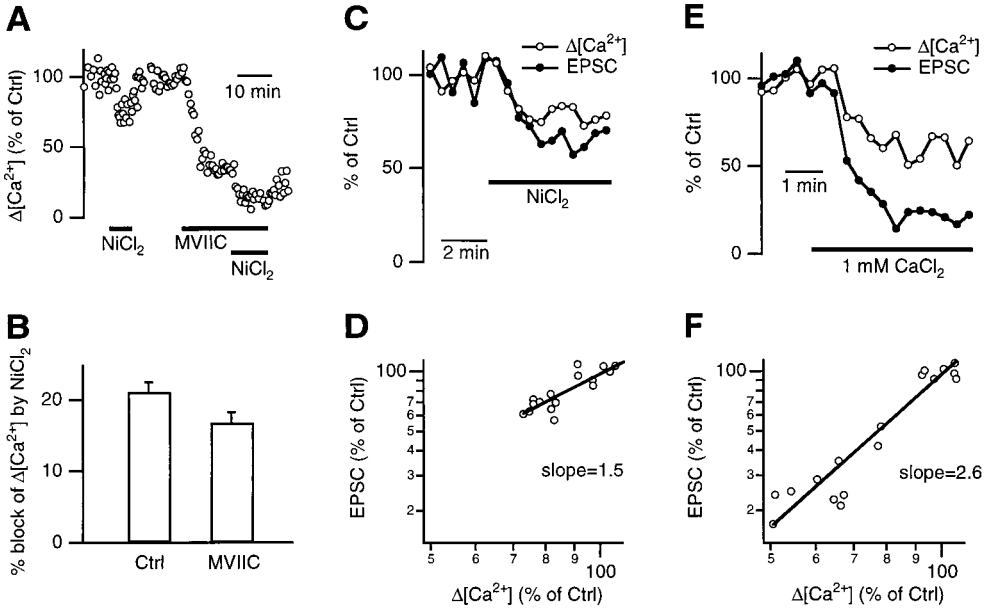

FIG. 3. R-type Ca^{2+} current mediates action-potential-evoked transmitter release with a lower efficacy. (*A*) $NiCl_2$ (100 μM) reversibly reduced $\Delta[Ca^{2+}]$ in control and in the presence of MVIIC in the same terminal. (*B*) Block of the $\Delta[Ca^{2+}]$ by 100 μM $NiCl_2$ in control ($n = 13$) and in the presence of MVIIC ($n = 7$). Percentages were normalized to values before drug application. (*C*) Application of 100 μM $NiCl_2$ simultaneously reduced the EPSC and the $\Delta[Ca^{2+}]$. (*D*) EPSCs plotted against the $\Delta[Ca^{2+}]$ from *C* on double logarithmic scales. The slope of the linear regression line was 1.5. (*E* and *F*) Similar plots as *C* and *D*, respectively, but with a decrease of the extracellular $CaCl_2$ concentration from 2 to 1 mM by substitution with $MgCl_2$. The slope of the regression line in *F* was 2.6.

The slope measured with application of $NiCl_2$ (1.4 ± 0.1) was significantly ($P < 0.01$, *t* test) smaller than that obtained with lowering $[Ca^{2+}]_o$ (2.7 ± 0.2) or with application of MVIIC (3.3 ± 0.3), suggesting a lower efficacy of R-type channels in controlling release. The mechanism underlying this observation is unclear. It is not caused by a difference in the Ca^{2+} current time course, because the kinetics of the R-type current evoked by action potential waveform commands was not significantly different from the total current (Fig. 2*B*). The location of the R-type Ca^{2+} channels at terminals might be important. For example, R-type channels could be located further away from the release sites than MVIIC-sensitive channels.

R-Type Current Is Inhibited by Activation of Presynaptic Metabotropic Glutamate Receptors and $GABA_B$ Receptors. Neurotransmitters and neuromodulators have been shown to cause presynaptic inhibition of evoked transmitter release primarily by inhibition of Ca^{2+} channels (see ref. 31 for review). Presynaptic inhibition may be a mechanism causing synaptic depression (31). To explore whether the R-type current is a target for presynaptic inhibition, we studied the effect of the $GABA_B$ receptor agonist baclofen (20 μM, Fig. 4*A*, $n = 4$) and the metabotropic glutamate receptor agonist L-AP4 (100 μM, Fig. 4*B*, $n = 4$). Both substances partially inhibited the R-type current (Fig. 4). Baclofen induced a slow phase in the activation of the R-type current (sample traces in Fig. 4*A*, $n = 4$), similar to G-protein-mediated modulation (32) of the α_{1E} current (33). Our results demonstrate direct modulation of presynaptic Ca^{2+} currents by activation of $GABA_B$ receptors.

In summary, we found that about one-quarter of the Ca^{2+} current evoked by a presynaptic action potential was carried by R-type current in MNTB synapses (Figs. 1 and 2). This current evokes transmitter release with a low efficacy (Fig. 3) and is modulated by neurotransmitters (Fig. 4), suggesting that it is a target for presynaptic inhibition of transmitter release. Because R-type channels control fast transmitter release with a lower efficacy than MVIIC-sensitive channels, they may contribute preferentially to mechanisms involving slower cytoplasmic calcium signaling, such as paired-pulse facilitation (34), posttetanic potentiation (34), and mobilization of synaptic vesicles (35). These findings may be of general significance because a significant fraction of presynaptic Ca^{2+} channels remained unidentified in a number of other synapses (3–5).

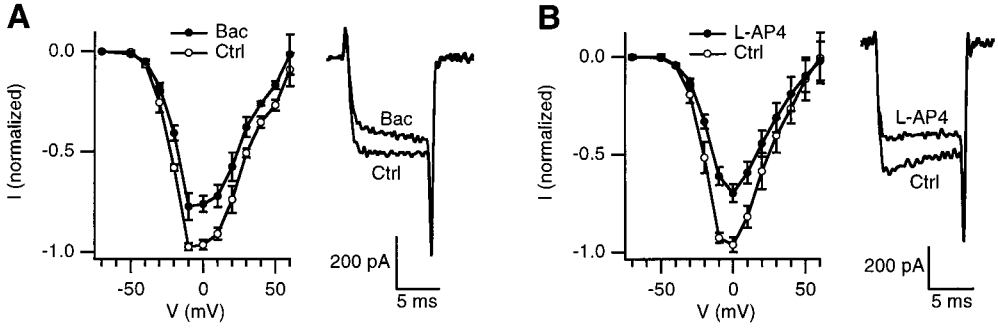

FIG. 4. Modulation of the R-type current by activation of $GABA_B$ or metabotropic glutamate receptors. *I–V* curves of the R-type current before (Ctrl) and after application of 20 μM baclofen ($n = 4$, *A*), or 100 μM L-AP4 ($n = 4$, *B*). Sample currents elicited at +10 mV before (Ctrl) and after drug application (*Right*, *A* and *B*). Experiments were performed in the presence of MVIIC.

We thank Drs. J. M. Bekkers and A. Reyes for helpful comments and Dr. W. Jarolimek for providing baclofen. This work was supported by the Alexander von Humboldt Foundation and Human Frontier Science Program to L.G.W. and a Training and Mobility of Researchers fellowship to J.G.G.B.

1. Dunlap, K., Luebke, J. I. & Turner, T. J. (1995) *Trends Neurosci.* **18,** 89–98.
2. Reuter, H. (1996) *Curr. Opin. Neurobiol.* **6,** 331–337.
3. Wu, L. G. & Saggau, P. (1995) *J. Neurophysiol.* **73,** 1965–1972.
4. Mintz, I., Sabatini, B. L. & Regehr, W. G. (1995) *Neuron* **15,** 675–688.
5. Turner, T. J., Lampe, R. A. & Dunlap, K. (1995) *Mol. Pharmacol.* **47,** 348–353.
6. Castillo, P. E., Weisskopf, M. G. & Nicoll, R. A. (1994) *Neuron* **12,** 261–269.
7. Wheeler, D. B., Randall, A. & Tsien, R. W. (1996) *J. Neurosci.* **16,** 2226–2237.
8. Luebke, J., Dunlap, K. & Turner, T. J. (1993) *Neuron* **11,** 895–902.
9. Takahashi, T. & Momiyama, A. (1993) *Nature (London)* **366,** 156–158.
10. Regehr, W. G. & Mintz, I. (1994) *Neuron* **12,** 605–613.
11. Zhang, J.-F., Randall, A. D., Ellinor, P. T., Horne, W. A., Sather, W. A., Tanabe, T., Schwarz, T. L. & Tsien, R. W. (1993) *Neuropharmacology* **32,** 1075–1088.
12. Randall, A. & Tsien, R. W. (1995) *J. Neurosci.* **15,** 2995–3012.
13. Borst, J. G. G., Helmchen, F. & Sakmann, B. (1995) *J. Physiol.* **489,** 825–840.
14. Takahashi, T., Forsythe, I. D., Tsujimoto, T., Barnes-Davies, M. & Onodera, K. (1996) *Science* **274,** 594–597.
15. Borst, J. G. G. & Sakmann, B. (1996) *Nature (London)* **383,** 431–434.
16. Borst, J. G. G. & Sakmann, B. (1998) *J. Physiol.* **506,** 143–157.
17. Borst, J. G. G. & Helmchen, F. (1998) in *Methods in Enzymology*, ed. Conn, P. M. (Academic, San Diego), Vol. 295, in press.
18. Grynkiewicz, G., Poenie, M. & Tsien, R. Y. (1985) *J. Biol. Chem.* **260,** 3440–3450.
19. Helmchen, F., Borst, J. G. G. & Sakmann, B. (1997) *Biophys. J.* **72,** 1458–1471.
20. Hillyard, D. R., Monje, V. D., Mintz, I., Bean, B. P., Nadasdi, L., Ramachandran, J., Miljanich, G., Azimi-Zoonooz, A., Mcintosh, J. M., Cruz, L. J., *et al.* (1992) *Neuron* **9,** 69–77.
21. McDonough, S. I., Swartz, K. J., Mintz, I. M., Boland, L. M. & Bean, B. P. (1996) *J. Neurosci.* **16,** 2612–2623.
22. Tottene, A., Moretti, A. & Pietrobon, D. (1996) *J. Neurosci.* **16,** 6353–6363.
23. Soong, T. W., Stea, A., Hodson, C. D., Dubel, S. J., Vincent, S. R. & Snutch, T. P. (1993) *Science* **260,** 1133–1136.
24. Williams, M. E., Marubio, L. M., Deal, C. R., Hans, M., Brust, P. F., Philipson, L. H., Miller, R. J., Johnson, E. C., Harpold, M. M. & Ellis, S. B. (1994) *J. Biol. Chem.* **269,** 22347–22357.
25. Fox, A. P., Nowicky, M. C. & Tsien, R. W. (1987) *J. Physiol.* **394,** 149–172.
26. Armstrong, C. M. & Matteson, D. R. (1985) *Science* **227,** 65–67.
27. Kaneda, M. & Akaike, N. (1989) *Brain Res.* **497,** 187–190.
28. Yu, B. & Shinnick-Gallagher, P. (1997) *J. Neurophysiol.* **77,** 690–701.
29. Olcese, R., Qin, N., Schneider, T., Neely, A., Wei, X., Stefani, E. & Birnbaumer, L. (1994) *Neuron* **13,** 1433–1438.
30. Stephens, G. J., Page, K. M., Burley, J. R., Berrow, N. S. & Dolphin, A. C. (1997) *Pflügers Arch.* **433,** 523–532.
31. Wu, L. G. & Saggau, P. (1997) *Trends Neurosci.* **20,** 204–212.
32. Hille, B. (1994) *Trends Neurosci.* **17,** 531–536.
33. Mehrke, G., Pereverzev, A., Grabsch, H., Hescheler, J. & Schneider, T. (1997) *FEBS Lett.* **408,** 261–270.
34. Kamiya, H. & Zucker, R. S. (1994) *Nature (London)* **371,** 603–606.
35. Heinemann, C., von Rüden, L., Chow, R. H. & Neher, E. (1993) *Pflügers Arch.* **424,** 105–112.
36. Wu, L.-G., Borst, J. G. G. & Sakmann, B. (1997) *Soc. Neurosci. Abstr.* **23,** 365.